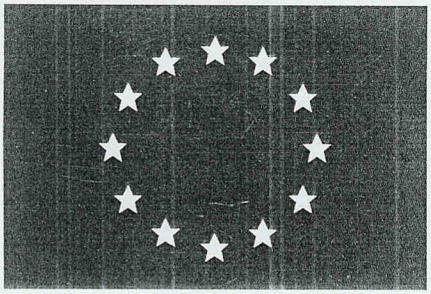

EUROPEAN COMMISSION

Gefördert vom

bmb+f

Bundesministerium für
Bildung, Wissenschaft,
Forschung und Technologie

Air pollution research report 56

Polar stratospheric ozone

Proceedings
of the
third European workshop
18 to 22 September 1995
Schliersee, Bavaria, Germany

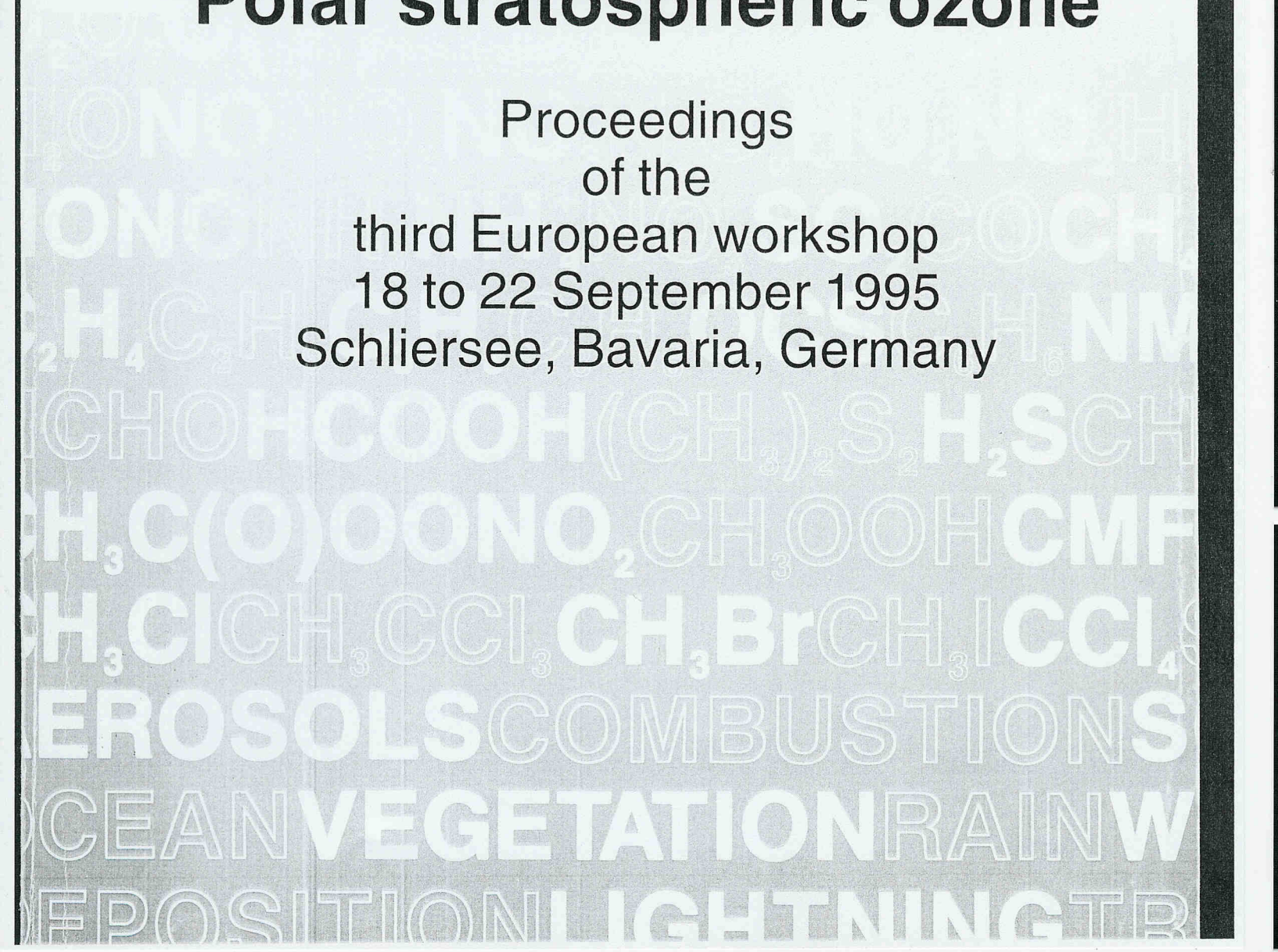

Presented at the Third European Symposium on Polar Stratospheric Ozone Research (Schliersee, Germany, 18-22 September 1995)

POLAR STRATOSPHERIC CLOUD OBSERVATIONS AT SODANKYLA (SF)

F. Masci
Istituto Nazionale di Geofisica, L'Aquila, Italy.
V. Rizi and G. Visconti
Dipartimento di Fisica, Università Degli Studi - L'Aquila, Italy.
C. Wedekind, F. Immler, B. Mielke, P. Rairoux, B. Stein, L. Woste
Freie Universitat Berlin, Berlin, Germany.
M. Del Guasta, M. Morandi, L. Stefanutti
IROE/CNR, Firenze, Italy
R. Matthey, V. Mitev
Observatorie Cantonal Neuchatel, Neuchatel, Swizerland
M. Douard, J. P. Wolf
Universitè Lyon, Villeurbanne, France
E. Kyro, R. Kivi
Finnish Meteorological Institute, Sodankyla, Finland

Introduction

We present some preliminary results of MOANA (Measurements and modelling of Ozone and Aerosols in the Northern Atmosphere) multi-wavelength lidar system, which was operating at Sodankyla (SF) during SESAME. We observed various polar stratospheric cloud (PSC) episodes; in this work we report the measurements of January 12 (J12) and January 19 (J19), 1995. The J12 PSC has a layered structure and two of the three particle layers show a depolarised backscattering signal. On the other hand the J19 PSC detected between 19 and 24km is likely composed of spherical (liquid) particles because no depolarization shows up. In the last case an analysis of the lidar backscattering at the different wavelengths allows to estimate the optical size distribution of the particles.

Aerosol Measurements

The MOANA lidar is a multi-wavelengths system: the Rayleigh elastic backscattering is detected at 355, 532, 750 and 1064nm channels (parallel), the Raman scattered radiation induced by the 355nm source is measured at 387nm, and two detection chains for the cross polarized backscattered radiation are available at 532 and 750nm (perpendicular). We analyse the backscattering signals at 355, 532 and 750nm channels. The aerosol backscattering ratio in both the parallel and perpendicular channels is defined as

$$R(z,\lambda) = 1 + \frac{\beta_a(z,\lambda)}{\beta_m(z,\lambda)}$$

z is the altitude, λ is the wavelength, $\beta_a(z,\lambda)$ and $\beta_m(z,\lambda)$ are respectively the aerosol and molecular backscattering coefficients.

The nearest PTU sounding obtained by the Finnish Meteorological Institute is used to calibrate the lidar molecular backscattering signals. Then the aerosol backscattering ratios have been calculated according to the method described in D'Altorio et al., (1993a). The aerosol depolarization is defined as:

$$\delta_a(z,\lambda) = \frac{\beta_a^{\,s}(z,\lambda)}{\beta_a^{\,s}(z,\lambda) + \beta_a^{\,p}(z,\lambda)} = \frac{\left(R_s(z,\lambda)-1\right)\delta_m}{R_s(z,\lambda)\delta_m + R_p(z,\lambda)\left(1-\delta_m\right)-1}$$

where the molecular depolarization , δ_m = 0.36 % (Wedekind et al , 1995), and (*s*) and (*p*) refer to the cross polarized and the parallel channels respectively.

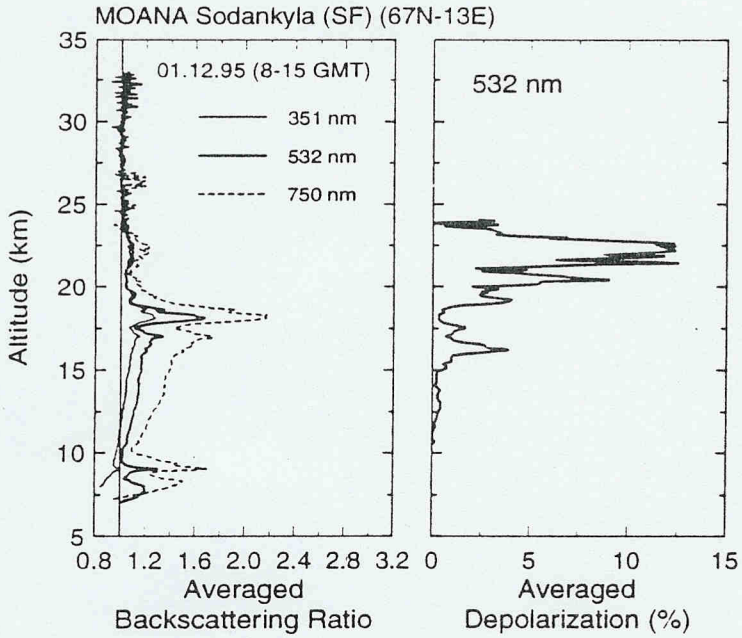

Figure 1. From left to right: the backscattering ratios at 355, 532, 750nm and the aerosol depolarization at 532nm. The backscattering ratios have been averaged along all the measurements taken between 08:00 GMT and 15:00 GMT

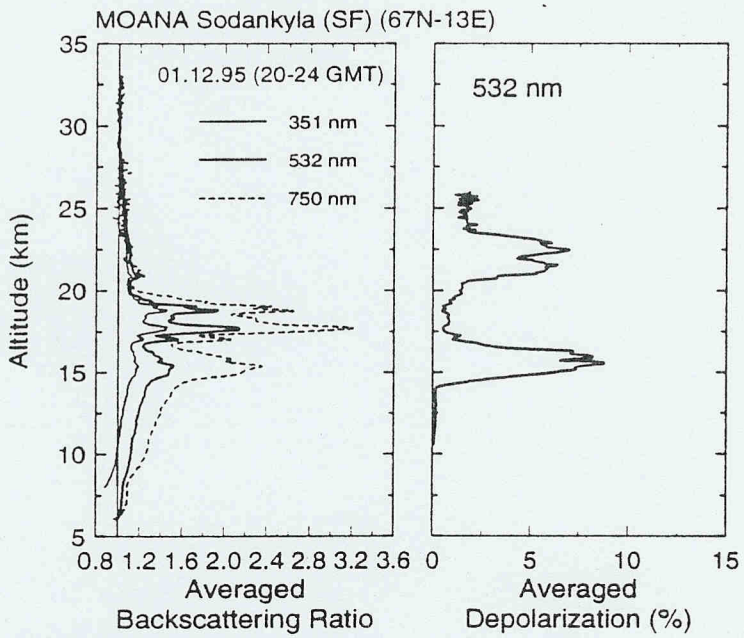

Figure 2. As Figure 1. The backscattering ratios have been averaged along all the measurements taken between 20:00 GMT and 24:00 GMT.

January 12, 1995 polar stratospheric cloud.

A PSC with a layered structure has been sampled in two different observation periods: from 08:00 to 14:00 GMT (period 1) and between 20:00 and 24:00 GMT (period 2). The backscattering ratio profiles averaged over period 1 and period 2 (Fig. 1, Fig. 2 and Fig. 3) allow to identify three main layers in the aerosol loading: between 14 and 17 km (layer 1), 18 and 21km (layer 2) and between 22

and 24 km (layer 3). From the period 1 to the period 2, the layer 1 shows a low increase in the aerosol loading, but the depolarization changes, suggesting the presence of solid aerosols during period 2. The layer 2 is constant in the backscattering ratio, on the other hand there is an evident decrease in the depolarization ratio during the period 2, this is the signature of a PSC made of liquid particles. The layer 3 does not evolve, but the depolarization values suggest that the particles remain solid during the observation periods.

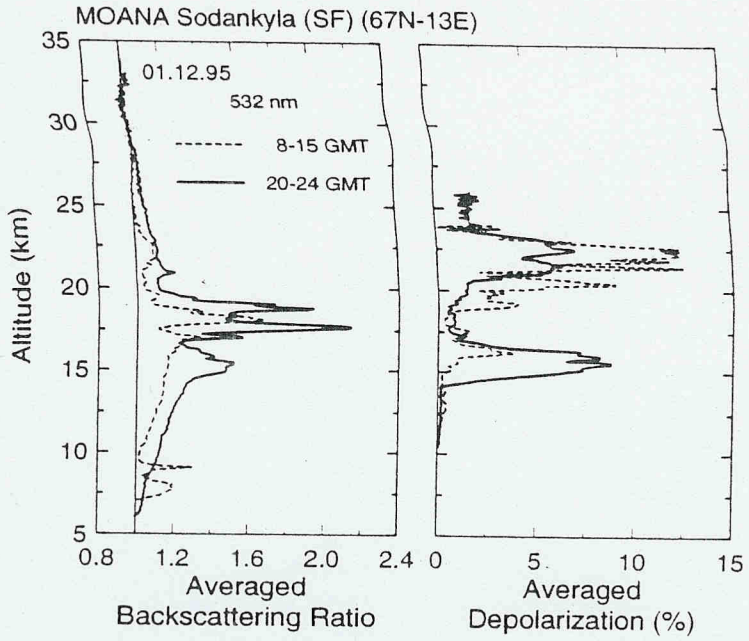

Figure 3. *The 532nm backscattering ratios and the aerosol depolarization averaged along the two time periods of the measurement session.*

We choose 400K (16.5km), 450K (19.0km) and 500K (21km) isentropic levels as those representative of the different PSC layers. The corresponding air mass back-trajectories are shown in Fig. 4 at two different arrival time: 10:00 GMT for period 1, and 22:00 GMT for period 2.

Before reaching the lidar site the air masses sampled at the different layers have performed quite low temperatures; then the observed liquid particles are likely $HNO_3/H_2SO_4/H_2O$ solution droplets and the solid aerosols should be poli-crystals made of nitric and/or sulfuric acid solid hydrates. We attempt to explain the observed temporal evolution of the different PSC layers according to the Koop et al., (1995) suggestions: the cold stratospheric particles made of nitric, sulfuric acid and water can form solid nitric acid and sulfuric acid hydrates after cooling below the frost point.

The appearance of solid particles in period 2 at layer 1 could be in agreement with Koop et al. freezing mechanism: the 400K air mass trajectory reaching the lidar site at 22:00 GMT cools down the frost point range 12hours before arriving, while the 10:00 GMT air mass remains above the ice freezing temperatures. Along the 10 days back-trajectories the air mass temperatures are always below the SAT melting threshold and well above the frost points.

The 450K 10:00 GMT and 22:00 GMT air mass thermal histories are similar in the last hours and 450K 22:00 GMT trajectory does not show the cooling needed for ice freezing; while the air mass sampled around 10:00 GMT performs temperatures next to the frost point 8 days before reaching the lidar site and the next thermal history never reaches the SAT melting region. These behaviours should be in agreement with the observations of solid particles in period 1 and liquid particles in period 2, assuming that the particles were liquid 10 days before LIDAR sampling.

The layer 3 solid particles show constant features along period 1 and 2; and the frozen state of these aerosols could be justified observing that the air mass cools below the frost point along 500K 10:00 GMT trajectory 6 days before lidar sampling, never reaching the SAT melting temperatures, on the other hand the 500K 22:00 GMT air mass has been exposed to temperatures below the frost point at

the beginning of the 10 days thermal history, and the following heating near to the SAT melting region has not changed the frozen state of the particles.

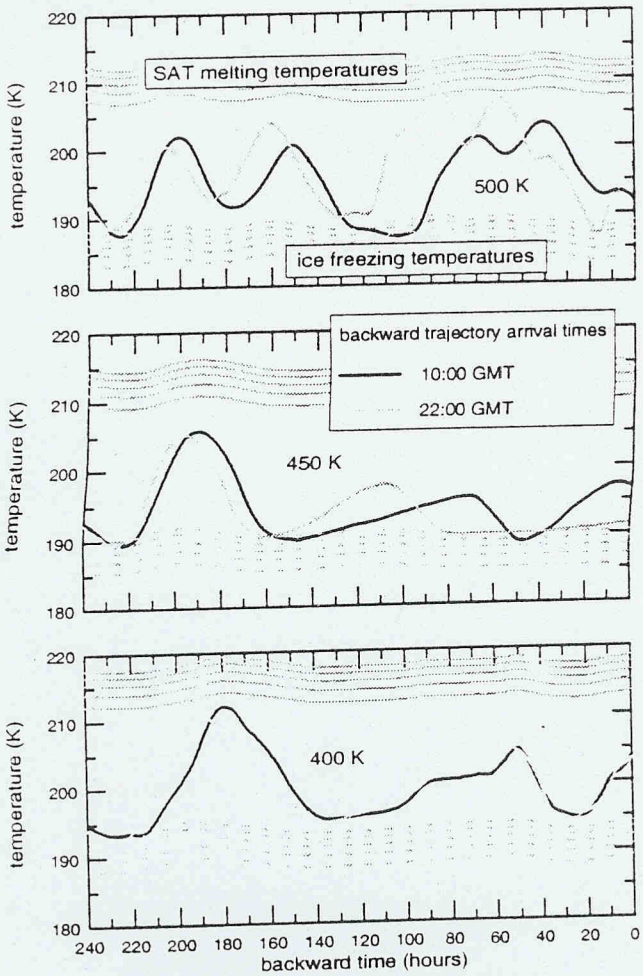

Figure 4. The air mass thermal histories representative of the three PSC layer observed on January 12, 1995 in period 1 (10:00 GMT) and in period 2 (22:00 GMT). The SAT melting temperatures (Zhang et al., 1993) and the water ice saturation temperature are also shown for a water content between 3ppmv (lower temperatures and 7ppmv (higher temperatures).

January 19, 1995 polar stratospheric cloud.

In this session of measurements a single PSC layer has been sampled by the MOANA lidar, this PSC is confined between 17 and 25km altitude range during the whole measurement session (10:00 GMT-20:00 GMT).

The time averaged backscattering ratio profiles and the aerosol depolarization are reported in Fig. 5, the depolarization measurements are below the lidar detection limit, indicating that the cloud is made of spherical (liquid) particles.

The thermal history of the sampled PSC air mass is discussed in Rizi et al., (1995): the temperature evolution is consistent with the formation of liquid $HNO_3/H_2SO_4/H_2O$ solution particles.

For the J19 PSC, we have retrieved some optical and size properties of the particles using the multi-wavelengths fitting algorithm described in D'Altorio et al., (1993b). By imposing that the PSC particles are represented with a log-normal size distribution, the lidar backscattering ratios are well fitted with a size distribution with a median radius $r_o = 0.50 \pm 0.10$ μm, geometrical width $\sigma = 1.35 \pm 0.10$ and the total particle density is $N_o = (5.0 \pm 2.0)\ 10^6$ particles m^{-3} ; the better fitting has been obtained using an index of refraction which may correspond to one expected for a dilute solution of water, nitric acid and sulfuric acid (1.37, 1.35, 1.33 at 355, 532 and 750nm respectively).

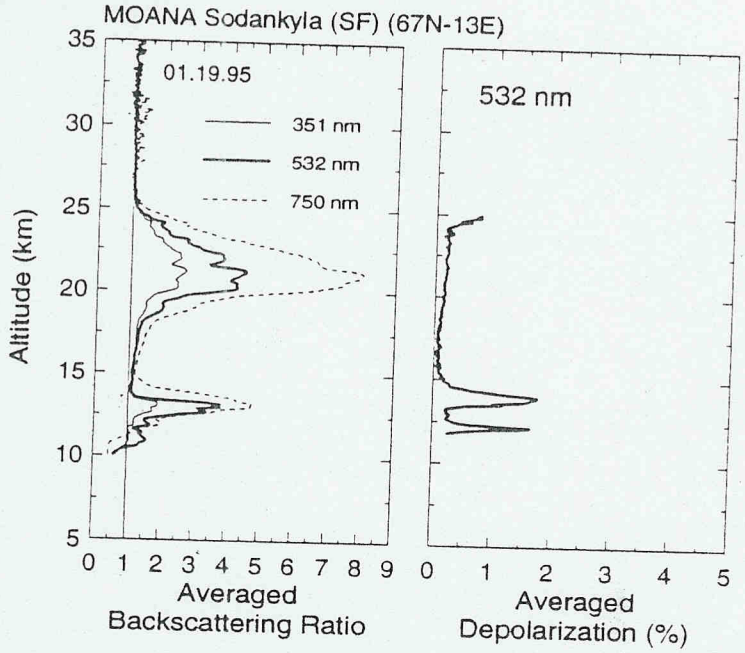

Figure 5. As Figure 1 and Figure 2. The backscattering ratios and the depolarization have been averaged along the measurement period (10:00 GMT - 20:00 GMT).

It must be stressed that the retrieved size distribution is optically equivalent to the sampled one; the lidar is sensitive to the aerosol backscattering coefficient, defined as:

$$\beta_a(z,\lambda) = \int_0^\infty dr\, n(r)\, Q_{bck}(r,\lambda)\, \pi r^2$$

where $Q_{bck}(r, \lambda)$ is the Mie backscattering efficiency, which is filtering the lidar sampled particles according to the radius. The shape of that size filter could be recalled by the plot of the function:

$$\int_0^r ds\, n(s)\, Q_{bck}(s,\lambda)\, \pi s^2$$

which is reported in Fig. 6 for λ = 532 nm and a log normal size distribution with total particle density $N_o = 10^7$ particles m^{-3}, median radius r_o = 0.1 μm and geometrical width σ = 2.0.

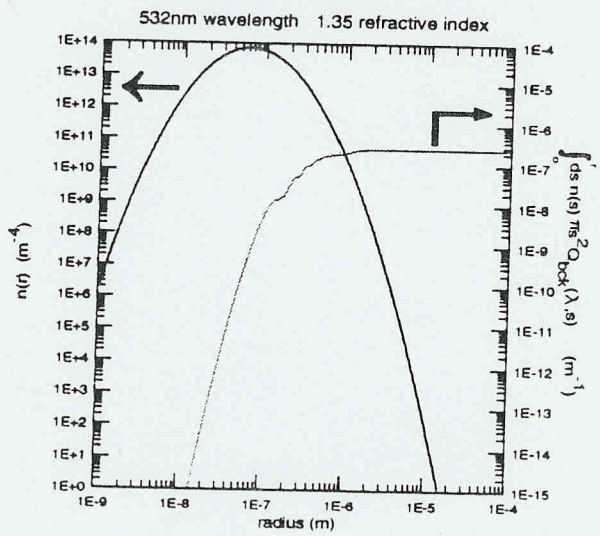

Figure 6. The sample size distribution (solid black line) and the cumulative aerosol backscattering coefficient (solid gray line) which evidences that the main contribution to lidar $\beta_a(\lambda, r)$ comes from larger particles.

In such example, only the particles with radius greater than 0.1 μm contribute to the aerosol backscattering ratio, then our optical fitting should give back a size distribution representing the

larger particles. In Rizi et al., (1995), the comparison between the optically retrieved size distribution and that simulated by a microphysical model is done accounting those lidar detection limits: we compare the lidar size distribution with the model one weighted with the Mie backscattering efficiency $Q_{bck}(\lambda,r)$.

References

D'Altorio et al., Continuos lidar measurements of stratospheric aerosol and ozone after the Pinatubo eruption. Part I: DIAL ozone retrieval in presence of stratospheric aerosol layers, *Geophys. Res. Lett.,20* ,2865-2868, 1993.

D'Altorio et al., Continuos lidar measurements of stratospheric aerosol and ozone after the Pinatubo eruption. Part II: Time evolution of ozone profiles and aerosol properties, *Geophys. Res. Lett., 20*, 2869-2872, 1993.

Koop et al., Do stratospheric aerosol droplets freeze above the ice frost point?, *Geophys. Res. Lett., 22*, 917-920, 1995.

Rizi et al.,Results of a trajectory box model simulating the size distribution evolution of stratospheric particles (sulfuric acid/water and sulfuric acid/nitric acid/water), *this issue*, 1995.

Wedekind et al.,.Lidar observations of liquid and solid PSC at Sodankyla, *this issue*, 1995.

Zhang et al., Physical chemistry of the H_2SO_4/H_2O binary system at low temperatures: Stratospheric implications, *J. Phys. Chem., 97*, 7351, 1993.